LETTERS

# The depolymerizing kinesin MCAK uses lattice diffusion to rapidly target microtubule ends

Jonne Helenius[1]*, Gary Brouhard[1]*, Yannis Kalaidzidis[1,2], Stefan Diez[1] & Jonathon Howard[1]

**The microtubule cytoskeleton is a dynamic structure in which the lengths of the microtubules are tightly regulated. One regulatory mechanism is the depolymerization of microtubules by motor proteins in the kinesin-13 family[1]. These proteins are crucial for the control of microtubule length in cell division[2–4], neuronal development[5] and interphase microtubule dynamics[6,7]. The mechanism by which kinesin-13 proteins depolymerize microtubules is poorly understood. A central question is how these proteins target to microtubule ends at rates exceeding those of standard enzyme–substrate kinetics[8]. To address this question we developed a single-molecule microscopy assay for MCAK, the founding member of the kinesin-13 family[9]. Here we show that MCAK moves along the microtubule lattice in a one-dimensional (1D) random walk. MCAK–microtubule interactions were transient: the average MCAK molecule diffused for 0.83 s with a diffusion coefficient of 0.38 $\mu m^2 s^{-1}$. Although the catalytic depolymerization by MCAK requires the hydrolysis of ATP, we found that the diffusion did not. The transient transition from three-dimensional diffusion to 1D diffusion corresponds to a "reduction in dimensionality"[10] that has been proposed as the search strategy by which DNA enzymes find specific binding sites[11]. We show that MCAK uses this strategy to target to both microtubule ends more rapidly than direct binding from solution.**

Kinesin-13 motor proteins act at microtubule ends, where they are thought to force protofilaments into a curved conformation[12,13], which is a likely structural intermediate in the depolymerization process[14]. Classically, kinesin motor proteins reach microtubule ends by ATP-dependent translocation along microtubules. However,

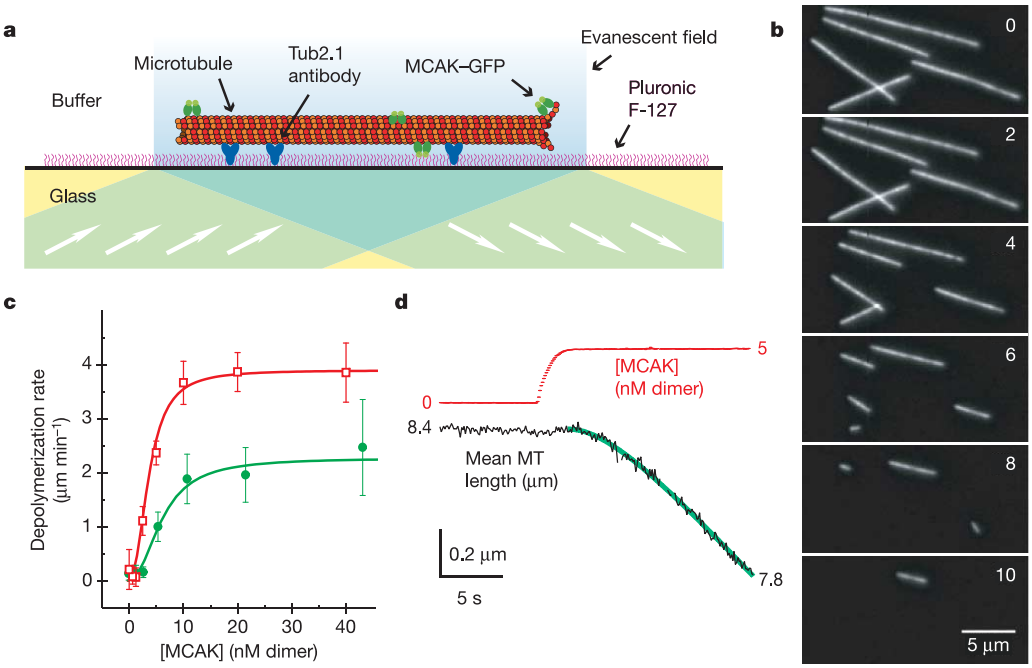


**Figure 1 | MCAK-dependent microtubule depolymerization. a**, Diagram of the *in vitro* assay depicting a microtubule (red) immobilized above the glass surface by anti-tubulin antibodies (dark blue). Excitation by total internal reflection allows the detection of single molecules (namely MCAK–GFP in green) in the evanescent field (shown in blue). **b**, Epifluorescence images of immobilized microtubules at the times shown in minutes. MCAK dimer (8 nM) was added at $t = 2$ min. **c**, Plot of microtubule depolymerization rate against MCAK concentration. Error bars are s.d. Data fitted to Hill equations (lines plotted) yielded $K_m = 3.9$ nM and $K_m = 6.1$ nM for MCAK and MCAK–GFP, and $n = 2.4$ and $n = 2.2$, respectively. Red squares, MCAK–$His_6$; green circles, MCAK–$His_6$–EGFP. **d**, Shortening of four microtubules from a mean length of 8.4 mm to 7.8 mm (black line) after the addition of 5 nM MCAK (red line). The depolymerization rate approached steady state with a time constant of 3.8 s (green fitted line).

[1]Max Planck Institute of Molecular Cell Biology and Genetics, Dresden 01307, Germany. [2]A. N. Belozersky Institute of Physico-Chemical Biology, Moscow State University, Moscow 119899, Russia.
*These authors contributed equally to this work.

directed motion has not been shown for kinesin-13 members[8]. To address the question of how kinesin-13 proteins reach microtubule ends, we expressed and purified two functional full-length versions of human MCAK: MCAK and green fluorescent protein (GFP)-tagged MCAK. We then developed a single-molecule microscopy assay for depolymerization (Fig. 1a) in which microtubules were immobilized on coverslips by means of surface-adsorbed anti-tubulin antibodies. Individual rhodamine-labelled microtubules and single MCAK–GFP molecules were revealed by epifluorescence and total-internal-reflection fluorescence (TIRF) illumination, respectively.

MCAK rapidly depolymerized GMP-CPP-stabilized microtubules in the depolymerization assay (Fig. 1b, and Supplementary movie 1). GMP-CPP (a slowly hydrolysable GTP analogue) was used to mimic the GTP found in the endcap of growing microtubules[15]. Depolymerization was ATP dependent and occurred at both microtubule ends. The depolymerization rate increased from its basal rate of $0.02\,\mu m\,min^{-1}$ to a peak rate of $3.9\,\mu m\,min^{-1}$ at 10 nM MCAK dimer (Fig. 1c). Thus, MCAK accelerated depolymerization up to 200-fold, with the maximum rate corresponding to about 50 tubulin dimers removed per second per microtubule end.

MCAK reached the microtubule ends very quickly. Microtubule lengths were measured after rapid infusion of MCAK into the observation chamber (Fig. 1d). On addition of 5 nM MCAK dimer, the depolymerization rate approached steady state with a rate constant, $k$, of $0.26\,s^{-1}$. This rate constant is related to the association rate to protofilament ends ($k_a = k[M]^{-1}$ when the MCAK concentration, [M], is much greater than the Michaelis constant, $K_m$), and $k_a$ must therefore be on the order of $50\,\mu M^{-1}\,s^{-1}$. Five experiments at either 5 or 10 nM MCAK gave an on-rate of $51 \pm 12\,\mu M^{-1}\,s^{-1}$ (results are means ± s.e.m. unless otherwise indicated). This confirms previous stopped-flow experiments[8]. Given that each microtubule has 14 protofilaments, we infer an association rate of about $700\,\mu M^{-1}\,s^{-1}$ to empty microtubule ends. These rates are significantly higher than expected for protein–protein association by three-dimensional diffusion in solution[16]; for example, the association of tubulin dimers onto the ends of growing microtubules occurs with an association rate of $2–5\,\mu M^{-1}\,s^{-1}$ (refs 16, 17).

These kinetic data suggest that the targeting of MCAK to the microtubule ends is somehow facilitated. To investigate this we performed experiments at MCAK–GFP concentrations that allowed single molecules to be observed (see Supplementary Information 1 for an analysis showing that single MCAK–GFP dimers were observed). Unlike other kinesins, which undergo directed movement on the microtubule lattice, we found that single MCAK–GFP molecules performed a random walk on the lattice during their transient interaction with a microtubule (Fig. 2a, and Supplementary movie 2). Using an in-house software package[18], we tracked 1,147 MCAK–microtubule interactions that lasted longer than 0.4 s and calculated the diffusion coefficient, $D$, of MCAK–GFP to be $0.38 \pm 0.01\,\mu m^2\,s^{-1}$ (Fig. 2b, Methods, and Supplementary Information 1). The interaction times were distributed exponentially (Fig. 2c), with a mean lifetime, $\langle t \rangle$, of $0.83 \pm 0.05$ s when corrected for photobleaching (Supplementary Information 1). At no time did we observe a directional bias in the diffusion (Supplementary Information 1).

The diffusion coefficient is high. Viewing diffusion as a random walk, the diffusion coefficient is related to the step size ($\delta$) and the time per step ($\tau$) by $D = \delta^2/2\tau$ (ref. 17). If $\delta = 8$ nm (corresponding to stepping between tubulin dimers along a protofilament), then $\tau = 0.084$ ms, implying that MCAK takes 12,000 diffusive steps per second. This is more than 100-fold faster than kinesin-1 steps directionally along the microtubule lattice[19].

To what extent does 1D diffusion increase the rate at which MCAK finds the ends of a microtubule? We calculated the average length scanned by MCAK during a diffusive interaction with a microtubule to be 0.79 μm, calculated as $\sqrt{(2D\langle t \rangle)}$. This length of microtubule adjacent to the end acts as an 'antenna' for MCAK molecules (see Supplementary Information 2). To estimate the flux of MCAK to the microtubule end, we write[20]

$$\frac{\partial c}{\partial t} = k_{on}C_m - k_{off}c + D\frac{\partial^2 c}{\partial x^2}$$

where $c(x,t)$ is the concentration of MCAK on the microtubule lattice at distance $x$ from the microtubule end and time $t$, $k_{on}$ is the attachment rate to the lattice, $C_m$ is the MCAK concentration in solution, and $k_{off}$ is the dissociation rate from the lattice. This equation excludes the contribution of the depolymerization rate, which is negligible. The steady-state solution of this equation is given by $c(x) = c_\infty(1 - e^{-x/x_0})$, where $c_\infty$ is the concentration on the microtubule lattice far from the end, in MCAK dimers per μm, and $x_0 = \sqrt{(D/k_{off})}$. The flux to the microtubule end is $J = -D\partial c/\partial x = -Dc_\infty/x_0$ (see Supplementary Information 3). $c_\infty$ was measured for MCAK–GFP concentrations of 0.3–3 nM by direct counting of molecules. This allowed us to calculate the attachment rate to the microtubule lattice, $k_{on} = 0.64 \pm 0.13\,nM^{-1}\,s^{-1}\,\mu m^{-1}$ ($n = 3$). With this value of $k_{on}$, we calculated a flux to the end of the microtubule of 2.2 MCAK–GFP dimers per second at 6 nM, corresponding to an association rate to protofilament ends of $k_a = 26\,\mu M^{-1}\,s^{-1}$. Thus, the diffusion of MCAK accounts theoretically for the very high association rate measured in the initial-rate experiments (Fig. 1d).

Diffusive scanning followed by end capture was directly observed, as shown in Fig. 3a (yellow arrowhead). If an MCAK–GFP molecule lands within 0.25 μm of the microtubule end, it is likely to diffuse to the end within our 100-ms frame acquisition time; this accounts for end-binding events not preceded by observable diffusion

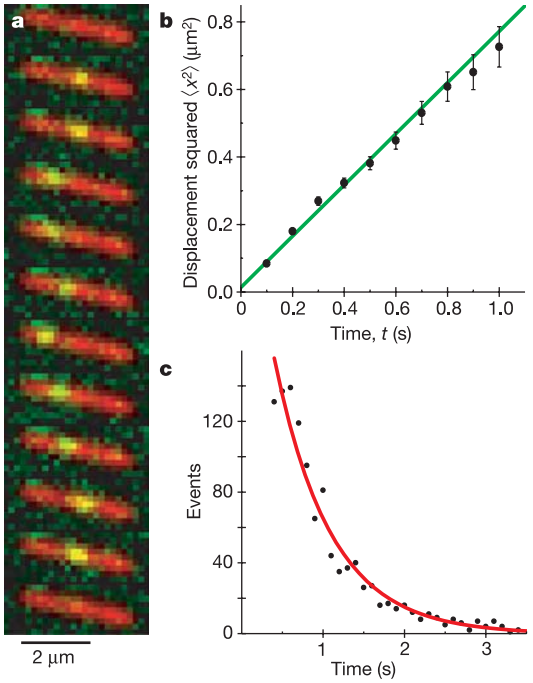


**Figure 2 | MCAK–GFP diffusion along microtubules.** **a**, Sequential frames of an MCAK–GFP (green) video. Twelve frames of a continuous TIRF-FITC recording (100-ms frames) were overlaid on one TRITC epifluorescence image of the microtubule (red). **b**, The mean-squared displacement of MCAK is plotted against the time interval over which it is measured. A linear curve fitted to the initial second yields a diffusion coefficient, $D$, of $0.38\,\mu m^2\,s^{-1}$; $\langle x^2 \rangle = 2Dt$. Error bars represent the s.e.m. of the squared displacement values. **c**, Histogram of durations of MCAK–GFP–microtubule interactions. An exponential curve fitted to the histogram (red) and corrected for photobleaching yields a mean lifetime of the interactions, $\langle t \rangle$, of 0.83 s.

(Fig. 3a, white arrowhead). Direct end binding from solution also occurs.

Why might MCAK use 1D diffusion instead of a directed walk to get to microtubule ends? One advantage is that, unlike directed motion, diffusion allows MCAK to target both ends of the microtubule, which is a significant feature of kinesin-13 localization *in vivo*[2,4]. A second advantage becomes clear when the diffusive movement of MCAK (with a diffusion coefficient of 0.38 $\mu m^2 s^{-1}$) is compared with the directed movement of kinesin-1 (with a velocity of 0.8 $\mu m\, s^{-1}$)[19]: MCAK covers shorter distances more rapidly (Fig. 3b). For any distance shorter than 1 $\mu$m, MCAK will outpace kinesin-1 in a race to the microtubule end.

We found evidence that the rapid diffusion of MCAK to the microtubule end does indeed accelerate the depolymerization reaction. First, increasing the KCl concentration from 75 mM to 125 mM greatly decreased the lifetime of MCAK on the microtubule lattice and decreased the depolymerization rate to baseline levels (Fig. 3c and Supplementary Information 4). Because a high salt concentration may disrupt direct end association as well as lattice diffusion, we did a second experiment in which the negatively charged carboxy termini of tubulin, known as the 'E-hook'[21], was removed by digestion with subtilisin. This prevented MCAK from diffusing on the lattice (Fig. 3d, e) and significantly decreased the depolymerization rate to 26 ± 3% of control microtubules ($P < 0.1\%$, Welch's *t*-test), as shown previously with microtubule sedimentation assays[12,13]. Direct end binding still occurred, and nearly maximum depolymerization rates were observed when using very high concentrations of MCAK (Supplementary Information 4). Therefore the decrease in depolymerization rate for subtilisin microtubules is best explained by a decrease in end-targeting caused by the lack of E-hook-mediated diffusion.

The electrostatic partner for the negatively charged E-hook is probably the positively charged 'neck' domain[22], which has been shown to be necessary for MCAK depolymerization activity *in vivo*[23]. Complementing earlier work showing that electrostatic interactions of positively charged regions of kinesin-1 (refs 24, 25) and kinesin-3 (ref. 26) with the E-hook enhance processivity of directed motility, our results indicate that these interactions are important for diffusive motility as well. Taken together, these data connect diffusion and depolymerization: electrostatic interactions between MCAK's neck domain and the E-hook of tubulin give rise to diffusion and accelerated depolymerization.

ATP is hydrolysed while MCAK interacts with the lattice of microtubules[8]. It is clear that each individual diffusive step does not require ATP hydrolysis, because MCAK's lattice-stimulated ATPase activity was previously measured to be only 1 $s^{-1}$ (ref. 8), much lower than the rate of diffusive stepping (12,000 $s^{-1}$). The mean interaction time of 0.83 s indicates that one diffusive interaction corresponds to one ATP hydrolysis cycle.

To determine whether diffusion depended on MCAK's nucleotide state, we performed single-molecule diffusion experiments with ADP, AMP-PNP (a non-hydrolysable ATP analogue) or apyrase (to digest all residual ATP and ADP) to mimic the ADP, ATP or

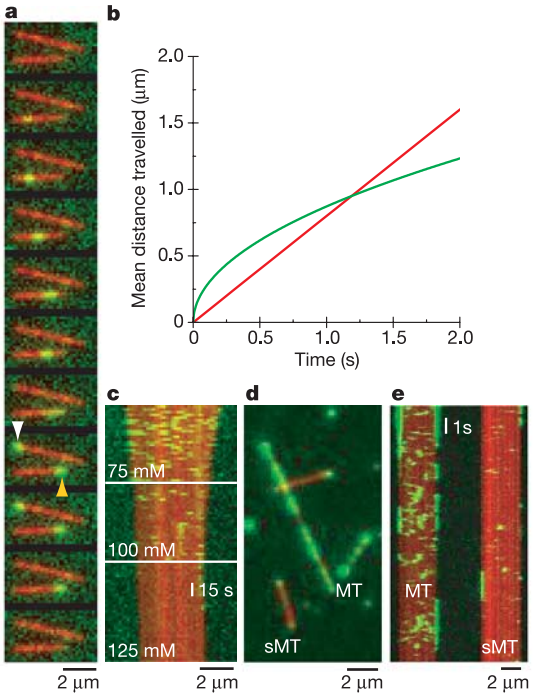


**Figure 3 | MCAK targeting of microtubule ends by means of diffusion.** **a**, Two MCAK–GFP molecules (green) interacting with separate microtubules (red) in 1 mM ATP (100-ms frames). Arrowheads indicate MCAK–microtubule end-binding events. **b**, Plot of average distance travelled over time by diffusing MCAK–GFP (green, $D = 0.38\,\mu m^2 s^{-1}$; $\langle x \rangle = \sqrt{(2Dt)}$) and walking kinesin-1 (red, velocity $v = 0.8\,\mu m\, s^{-1}$; $\langle x \rangle = vt$). **c**, Kymograph showing the effect of KCl concentration on the MCAK interaction with a single microtubule. Microtubules are depicted along the horizontal axis while time changes along the vertical axis. The MCAK and MCAK–GFP concentrations were 2.5 and 0.25 nM, respectively. **d**, Dual-colour image of normal microtubules (MT) and subtilisin-digested microtubules (sMT) in the presence of 3 nM MCAK–GFP (green). **e**, Kymographs showing diffusion on a normal microtubule (MT) and only brief binding/unbinding events on a subtilisin-digested microtubule (sMT) at about 1 nM MCAK–GFP.

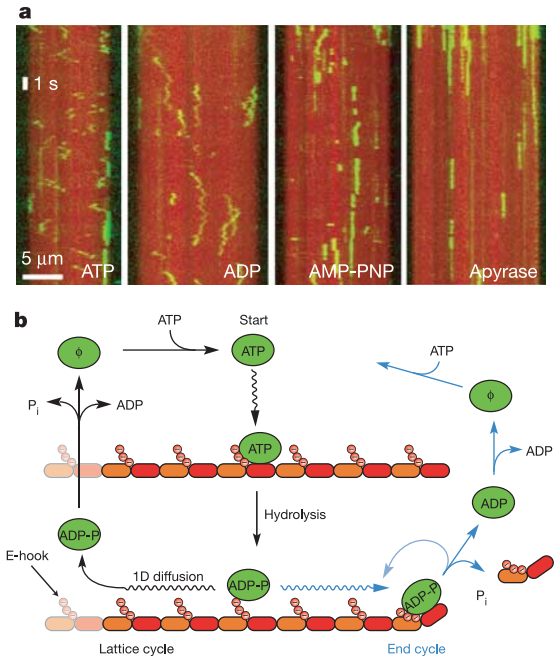


**Figure 4 | MCAK nucleotide states and diffusion model.** **a**, Kymographs depicting the motion of MCAK–GFP (green) along microtubules (red) in the presence of ATP (1 mM), ADP (1 mM), AMP-PNP (1 mM) and apyrase. The MCAK–GFP concentration was 0.6 nM except with apyrase, when it was 20 pM. **b**, MCAK–microtubule interaction model. Binding of soluble MCAK-ATP (green) induces rapid hydrolysis, accounting for the lattice-stimulated ATPase activity[8]. Next, MCAK-ADP-$P_i$ diffuses along the lattice by means of the E-hook of tubulin. It may disassociate, 'unproductively' completing the hydrolysis cycle (left, black arrows). Alternatively, it may reach a microtubule end, where the removal of tubulin dimers is coupled to $P_i$ release (right, blue arrows), accounting for the end-stimulated ATPase activity[8]. MCAK may detach from the end (straight blue arrow) or, if processive, may stay attached to remove additional dimers (light blue arrow).

nucleotide-free states, respectively. In 1 mM ADP, MCAK–GFP bound microtubules and moved in a diffusive manner ($D = 0.22 \pm 0.01\,\mu m^2\,s^{-1}$, $\langle t \rangle = 1.75 \pm 0.06$ s, $n = 1{,}076$) proving that diffusion occurred without energy derived from the hydrolysis of ATP (Fig. 4a, and Supplementary movie 3). Similar diffusion coefficients were measured in 0.1 and 10 mM ADP. The statistically significant difference in diffusion parameters ($D$ and $\langle t \rangle$) in ADP compared with ATP implies that, in the presence of ATP, MCAK does not primarily diffuse in the ADP state. MCAK-AMP-PNP could bind to microtubules but only rarely showed diffusive steps ($D = 0.014\,\mu m^2\,s^{-1}$, $\langle t \rangle = 3.5$ s). When apyrase was added to remove both ATP and ADP from solution enzymatically, nucleotide-free MCAK–GFP went into a rigor state with greatly reduced diffusion ($D = 0.003\,\mu m^2\,s^{-1}$, $\langle t \rangle = 3.9$ s).

In the presence of ATP, MCAK must diffuse in one or more of the four possible nucleotide states: nucleotide-free, ATP, ADP and ADP-$P_i$. As MCAK binds tightly in the presence of AMP-PNP and apyrase, both the ATP and nucleotide-free states are excluded. Because the diffusion observed in ADP is statistically distinct from that observed in ATP, MCAK apparently diffuses in the ADP-$P_i$ state. To induce an ADP-$P_i$-like state, we performed a single-molecule diffusion experiment in ADP·$AlF_x$, ADP·$BeF_x$ and ADP·vanadate. Diffusion was observed in all three cases (Supplementary Information 5). The results imply that MCAK normally, in the presence of ATP, diffuses in the ADP-$P_i$ state.

In what nucleotide state is MCAK when it first encounters the microtubule? To determine the nucleotide state of soluble MCAK, we measured the amounts of radiolabelled α- and γ-phosphates of ATP bound to MCAK and kinesin-1 free in solution without microtubules (Supplementary Information 5). As shown previously[27], no γ-$P_i$ was bound to kinesin (γ-$P_i$/α-$P_i$ = −11 ± 8% in two experiments). However, equal amounts of α-$P_i$ and γ-$P_i$ remained bound to MCAK (γ-$P_i$/α-$P_i$ = 116 ± 11% in three experiments). This shows that MCAK exists in the ATP or ADP-$P_i$ state in solution, unlike kinesin-1, and indicates that the functional differences between kinesin-1 and kinesin-13 family proteins are achieved through differences in hydrolysis mechanisms. The nucleotide data were used to formulate a MCAK–microtubule interaction model that accounts for both the microtubule lattice-stimulated and end-stimulated ATPase activity of MCAK (Fig. 4b).

After arriving at the end, each MCAK seems to remove several dimers. Comparison of the flux to the microtubule end calculated theoretically (2.2 MCAK dimers per second at 6 nM) with the off-rate of tubulin dimers ($14\,s^{-1}$ at 6 nM MCAK–GFP) indicates that each MCAK removes about seven tubulin dimers for each end-targeting event. On average, single MCAK end-binding events were observed to last 1.9 ± 0.2 s ($n = 239$, corrected for photobleaching). At saturating concentration, MCAK removes tubulin dimers from protofilaments at a rate of two dimers per second, so an MCAK that resides for 1.9 s at an end would remove about four tubulin dimers. Taken together, these results indicate that MCAK might act processively at the microtubule end.

By diffusing along microtubules instead of walking, MCAK rapidly targets both microtubule ends. A comparable process is the rapid targeting of DNA restriction enzymes to their restriction sites, which also exceeds the three-dimensional diffusion limit[28]. These DNA enzymes are thought to target their restriction sites by a 1D diffusional scan of DNA segments[29,30], but this search mechanism has not been observed at the single-molecule level. Here we have characterized the 1D diffusion of MCAK on microtubules and shown the implications of this diffusion for end targeting. The single-molecule data presented here support the 'reduction in dimensionality' hypothesis.

The MCAK neck domain data[23] suggest that 1D diffusion operates *in vivo* to target MCAK to microtubule ends. Once at the ends, MCAK and its homologues interact with other proteins, such as the plus-end-binding proteins XMAP215 and EB1 (refs 6, 7), to regulate microtubule dynamics. The *in vitro* single-molecule approach taken here could be useful to study the dynamics of this molecular machinery.

## METHODS

**Proteins.** Human MCAK–$His_6$ and human MCAK–$His_6$ tagged with enhanced GFP were expressed in *Spodoptera frugiperda* (Sf9) cells (BAC-TO-BAC expression system; Invitrogen) and purified by cation-exchange, metal-chelating, and desalting or gel-filtration chromatography. Most experiments with MCAK–GFP were performed with freshly purified protein. A filter-based radiometric ATP binding assay[8] with [γ-$^{32}$P]ATP and [α-$^{32}$P]ATP was used to determine the concentration of active MCAK and the nucleotide state of proteins in solution. Details are given in Supplementary Information 5 and 6. Reagents were purchased from Sigma unless indicated otherwise. Pig-brain tubulin was purified, rhodamine-labelled (TAMRA; Invitrogen) and polymerized with GMP-CPP (Jena Bioscience) as described previously[8]. Key experiments were repeated with Taxol-stabilized microtubules; no differences were observed. Digestion was performed with $10\,\mu g\,ml^{-1}$ subtilisin, incubated for 20 min at 37 °C, and terminated with 2 mM phenylmethylsulphonyl fluoride.

**Imaging.** Images were acquired with either a Roper Scientific MicroMAX:512BFT charge-coupled device camera or an Andor DV887 iXon camera with Zeiss Axiovert 200M microscopes and Zeiss 100 × /1.45 α Plan-FLUAR objectives. The microscopes were outfitted with a dual-port TIRF condenser (Till Photonics) or a prototype VisiTIRF condenser (Visitron Systems). Fluorescein isothiocyanate (FITC) and tetramethylrhodamine β-isothiocyanate (TRITC) filter sets (Chroma Technology Corp.) were used to image GFP (TIRF) and TAMRA (epifluorescence) fluorophores, respectively. The standard exposure time was 100 ms.

**Depolymerization assay.** Microscope chambers were constructed with 18 mm × 18 mm and 22 mm × 22 mm coverslips separated by double-sided tape (Scotch 3M) to create channels 0.1 mm thick, 3 mm wide and 18 mm long. Glass coverslips (no. 1.5; Corning) were cleaned in Pirnaha solution ($H_2O_2/H_2SO_4$, 3:5) before silanization in 0.05% dichlorodimethylsilane in trichloroethylene. Detailed methods are given in Supplementary Information 6. To immobilize microtubules, channels were incubated with 0.2% Tub 2.1 antibody in BRB80 for 5 min, followed by 5 min with 1% Pluronic F-127 in BRB80, and finally GMP-CPP microtubules in BRB80 for 15 min. Channels were rinsed with BRB20 (20 mM PIPES-/KOH pH 6.9, 1 mM $MgCl_2$, 1 mM EGTA) before addition of the imaging solution (BRB20 supplemented with 75 mM KCl, $0.1\,mg\,ml^{-1}$ BSA, 1 mM ATP or other nucleotides, 1% 2-mercaptoethanol, 40 mM glucose, $40\,\mu g\,ml^{-1}$ glucose oxidase, $16\,\mu g\,ml^{-1}$ catalase, and MCAK).

**Imaging analysis.** The Motion Tracking software package, written in the Pluk development environment, was used to locate and track MCAK–GFP molecules[18]. The validity of each track was confirmed by visual inspection. The Pluk-derived diffusion coefficient was cross-checked against, first, trajectories generated by hand with kymographs and a custom MATLAB-based two-dimensional gaussian peak-fitting tool, and second, an analysis of displacement distributions that does not require manual inspection. Details are given in Supplementary Information 1. For each condition examined, at least three separate experiments were performed, and multiple films of each experiment were analysed, yielding no less than 100 molecules.

**Received 16 February; accepted 17 March 2006.**

1. Desai, A., Verma, S., Mitchison, T. J. & Walczak, C. E. Kin I kinesins are microtubule-destabilizing enzymes. *Cell* **96**, 69–78 (1999).
2. Maney, T., Hunter, A. W., Wagenbach, M. & Wordeman, L. Mitotic centromere-associated kinesin is important for anaphase chromosome segregation. *J. Cell Biol.* **142**, 787–801 (1998).
3. Rogers, G. C. *et al.* Two mitotic kinesins cooperate to drive sister chromatid separation during anaphase. *Nature* **427**, 364–370 (2004).
4. Walczak, C. E., Mitchison, T. J. & Desai, A. XKCM1: a *Xenopus* kinesin-related protein that regulates microtubule dynamics during mitotic spindle assembly. *Cell* **84**, 37–47 (1996).
5. Homma, N. *et al.* Kinesin superfamily protein 2A (KIF2A) functions in suppression of collateral branch extension. *Cell* **114**, 229–239 (2003).
6. Tournebize, R. *et al.* Control of microtubule dynamics by the antagonistic activities of XMAP215 and XKCM1 in *Xenopus* egg extracts. *Nature Cell Biol.* **2**, 13–19 (2000).
7. Mennella, V. *et al.* Functionally distinct kinesin-13 family members cooperate to regulate microtubule dynamics during interphase. *Nature Cell Biol.* **7**, 235–245 (2005).
8. Hunter, A. W. *et al.* The kinesin-related protein MCAK is a microtubule depolymerase that forms an ATP-hydrolyzing complex at microtubule ends. *Mol. Cell* **11**, 445–457 (2003).

9. Wordeman, L. & Mitchison, T. J. Identification and partial characterization of mitotic centromere-associated kinesin, a kinesin-related protein that associates with centromeres during mitosis. *J. Cell Biol.* **128,** 95–104 (1995).
10. Adam, G. & Delbruck, M. in *Structural Chemistry of Molecular Biology* (eds Rich, A. & Davidson, N.) 198–215 (Freeman, San Francisco, 1968).
11. Richter, P. H. & Eigen, M. Diffusion controlled reaction rates in spheroidal geometry. Application to repressor–operator association and membrane bound enzymes. *Biophys. Chem.* **2,** 255–263 (1974).
12. Moores, C. A. *et al.* A mechanism for microtubule depolymerization by KinI kinesins. *Mol. Cell* **9,** 903–909 (2002).
13. Niederstrasser, H., Salehi-Had, H., Gan, E. C., Walczak, C. & Nogales, E. XKCM1 acts on a single protofilament and requires the C terminus of tubulin. *J. Mol. Biol.* **316,** 817–828 (2002).
14. Mandelkow, E. M., Mandelkow, E. & Milligan, R. A. Microtubule dynamics and microtubule caps: a time-resolved cryo-electron microscopy study. *J. Cell Biol.* **114,** 977–991 (1991).
15. Hyman, A. A., Salser, S., Drechsel, D. N., Unwin, N. & Mitchison, T. J. Role of GTP hydrolysis in microtubule dynamics: information from a slowly hydrolyzable analogue, GMPCPP. *Mol. Biol. Cell* **3,** 1155–1167 (1992).
16. Northrup, S. H. & Erickson, H. P. Kinetics of protein–protein association explained by Brownian dynamics computer simulation. *Proc. Natl Acad. Sci. USA* **89,** 3338–3342 (1992).
17. Howard, J. *Mechanics of Motor Proteins and the Cytoskeleton* (Sinauer, Sunderland, Massachusetts, 2001).
18. Kalaidzidis, Y. L., Gavrilov, A. V., Zaitsev, P. V., Kalaidzidis, A. L. & Korolev, E. V. PLUK—an environment for software development. *Program. Comput. Softw.* **23,** 206–211 (1997).
19. Howard, J., Hudspeth, A. J. & Vale, R. D. Movement of microtubules by single kinesin molecules. *Nature* **342,** 154–158 (1989).
20. Klein, G. A., Kruse, K., Cuniberti, G. & Julicher, F. Filament depolymerization by motor molecules. *Phys. Rev. Lett.* **94,** 108102 (2005).
21. Paschal, B. M., Obar, R. A. & Vallee, R. B. Interaction of brain cytoplasmic dynein and MAP2 with a common sequence at the C terminus of tubulin. *Nature* **342,** 569–572 (1989).
22. Maney, T., Wagenbach, M. & Wordeman, L. Molecular dissection of the microtubule depolymerizing activity of mitotic centromere-associated kinesin. *J. Biol. Chem.* **276,** 34753–34758 (2001).
23. Ovechkina, Y., Wagenbach, M. & Wordeman, L. K-loop insertion restores microtubule depolymerizing activity of a 'neckless' MCAK mutant. *J. Cell Biol.* **159,** 557–562 (2002).
24. Thorn, K. S., Ubersax, J. A. & Vale, R. D. Engineering the processive run length of the kinesin motor. *J. Cell Biol.* **151,** 1093–1100 (2000).
25. Wang, Z. & Sheetz, M. P. The C-terminus of tubulin increases cytoplasmic dynein and kinesin processivity. *Biophys. J.* **78,** 1955–1964 (2000).
26. Nitta, R., Kikkawa, M., Okada, Y. & Hirokawa, N. KIF1A alternately uses two loops to bind microtubules. *Science* **305,** 678–683 (2004).
27. Hackney, D. D. Kinesin ATPase: Rate-limiting ADP release. *Proc. Natl Acad. Sci. USA* **85,** 6314–6318 (1988).
28. Riggs, A. D., Bourgeois, S. & Cohn, M. The lac repressor–operator interaction. 3. Kinetic studies. *J. Mol. Biol.* **53,** 401–417 (1970).
29. Winter, R. B., Berg, O. G. & von Hippel, P. H. Diffusion-driven mechanisms of protein translocation on nucleic acids. 3. The *Escherichia coli* lac repressor–operator interaction: kinetic measurements and conclusions. *Biochemistry* **20,** 6961–6977 (1981).
30. Halford, S. E. & Marko, J. F. How do site-specific DNA-binding proteins find their targets? *Nucleic Acids Res.* **32,** 3040–3052 (2004).


**Supplementary Information** is linked to the online version of the paper at www.nature.com/nature.

**Acknowledgements** We thank R. Hartmann for cloning and protein purification work; V. Varga for purification of unlabelled MCAK; E. Schäffer for the application of F-127; F. Ruhnow for the two-dimensional gaussian peak-fitting tool; A. Hyman, F. Jülicher, E. Schäffer, I. Riedel, J. Stear, G. Klein, V. Varga, A. Hunt and H. T. Schek for review of the manuscript; and S. Wolfson for proofreading and editing. Andor Technologies lent us the Andor iXon camera, and the VisiTIRF condenser was developed in collaboration with Visitron Imaging Systems, GmbH. This research was supported by the Max Planck Gesellschaft and the NIH.

**Author Information** Reprints and permissions information is available at npg.nature.com/reprintsandpermissions. The authors declare no competing financial interests. Correspondence and requests for materials should be addressed to J.H. (howard@mpi-cbg.de).